Lithium plasmon based low-powered dynamic color display

Jie Liang[1, †], Yan Jin[1, †], Huiling Yu[1], Xinjie Chen[1], Lin Zhou[1, *], Pengcheng Huo[1], Ye Zhang[1], Haiyang Ma[1], Yi Jiang[1], Bin Zhu[1], Ting Xu[1], Hui Liu[1], Shining Zhu[1] and Jia Zhu[1, *]

[1] National Laboratory of Solid State Microstructures, College of Engineering and Applied Sciences, School of Physics, Key Laboratory of Intelligent Optical Sensing and Manipulation, Ministry of Education, Jiangsu Key Laboratory of Artificial Functional Materials, Nanjing University, Nanjing 210093, China.

***Corresponding authors.** E-mails: linzhou@nju.edu.cn; jiazhu@nju.edu.cn

[†] These authors contributed equally to this work.

ABSTRACT

Display and power supply have been two essential and independent cornerstones of modern electronics. Here we report a lithium plasmon based low-powered dynamic color display with intrinsic dual functionalities, the plasmonic display and energy recycling unit, through the electric-driven transformation of nanostructured lithium metals. Dynamic color displays are enabled by plasmonic transformation through electrodeposition (electrostripping) of the lithium metals during the charging (discharging) processes, while the consumed energy for coloring can be retrieved in the inverse processes respectively. The energy recycling of lithium metals makes the energy consumption of the display device down to 0.390 mW cm^{-2} (0.105 mW cm^{-2}) for the active (static) coloration state of a proof-of-concept display/battery device, which approaches nearly-zero-energy-consumption towards the near-100%-energy-efficiency limit of commercial lithium batteries. Combining the subwavelength feature of plasmonics with the effective energy recycling, the lithium plasmon based dynamic display offers a promising route towards next-generation integrated photonic devices, with intriguing advantages of low energy consumption, small footprint and high resolution.

Keywords:

lithium plasmon, dynamic display, lithium metal battery, low energy consumption, lithium nanoparticle

INTRODUCTION

Display and power supply are two essential and independent building blocks to support the development of modern electronics [1-5]. Driven by premier applications ranging from portable mobile electronics to large-scale indoor and/or outdoor billboards, displays and batteries have evidenced significant advancements in the past centuries, independently. For next-generation mobile devices, both low-energy-consumption display modules beating organic light emitting displays technologies (>10 mW cm^{-2}) and high-energy-density portable batteries are urgently needed [6-12]. While displays and batteries need to work seamlessly, as displays consume a significant portiopin (up to 68%) of power for electronics [13-16], the development paths of the two fields have never converged thus far.

Alkali metals are attracting significant attention at the intersection of plasmonics and energy storage [17-19]. On the one hand, the alkali metal is emerging as a low loss and active plasmonic material [19-22]. Plasmonics, with the unique capability of focusing light into subwavelength scale, offers a promising solution for high-resolution display [23-28], featuring prominently compared with other structure color materials like all-dielectric metasurfaces, semiconductors and phase change materials [29-35]. In addition, external electrical (such as nanostructured noble metal deposition [36]), chemical or other stimuluses can be more effective to enable dynamic displays with respect to dielectric-based nanophotonic counterparts [37-46]. On the other hand, as the lightest metal, lithium (Li) metal has long been regarded as the holy grail of high-energy-density anode materials [10,12], with the high specific capacity (3860 mAh g^{-1}) and the lowest electrochemical potential (−3.04 V versus the standard hydrogen electrode).

Here for the first time, we demonstrate a Li metal-based low-powered dynamic plasmonic color display, which is simultaneously a nanostructured anode of a Li metal battery, with therefore inherited advantages of the dynamic tunability and extremely low energy consumption.

During the charging process, Li metal nucleates and grows on a pre-patterned substrate, resulting in the generation and tuning of plasmonic colors. During the discharging process, Li metal strips off from the substrate, thus leading to the erasing of the color.

The energy storage feature of Li metal enables effective energy recycling and reduces the overall energy consumption down to 0.390 mW cm^{-2} for the active coloration state and 0.105 mW cm^{-2} for the static coloration state of a proof-of-concept display/battery device, vital for energy-efficient display technologies. The dual functionalities of the display and power supplies enable a low-powered display device, in which one charged pixel can power another one to release its energy and vice versa during repeated cycling. Our results may offer a unique opportunity for the nano-scaled integrated platform for energy storage and information display.

RESULTS AND DISCUSSION

The schematic of the low-powered dynamic plasmonic color display

The schematic of the low-powered dynamic color display of plasmonic lithium metals is illustrated in Fig. 1a, which behaves as a planar Li metal battery instantaneously (see METHODS and Supplementary Fig. 1 for fabrication details, see the optical photograph and scanning electron microscope (SEM) images of the integrated display unit in Supplementary Fig. 2). Since the display panel is also a battery, it is composed of a Li source ($LiFePO_4$) as the cathode and a perforated magnesium fluoride (MgF_2) film on tungsten (W) as the anode template with liquid electrolyte as the ambience. Note that the pre-patterned anode template with the periodically perforated MgF_2 film (the period *p*, the diameter of hole *h,* see magnified schematic in the top panel of Fig. 1a) is originally at the colorless “off” state.

Serving as both core elements of color pixels for display and anodes for battery, the microstructure of Li nanoparticles is electrically programmable by the electrochemical reactions.

During the charging process, as a charging current is applied, Li ions from the cathode ($LiFePO_4$) migrate towards the pre-patterned anode template. Once these Li ions are reduced at the target sites, Li metal nucleates and electrodeposits into the pre-patterned holes of the MgF_2 film, forming the well-defined nano-hemispheres (diameter *d*, see schematic in the bottom panel of Fig. 1a) that serve as the reflective pixel units of the colorful "on" state. Note that the electric-driven redox reaction of the battery is reversible. During the discharging process, the deposited Li metal nanoparticles can be removed from the holes of the anode and reset the colorful display back to a colorless "off" state.

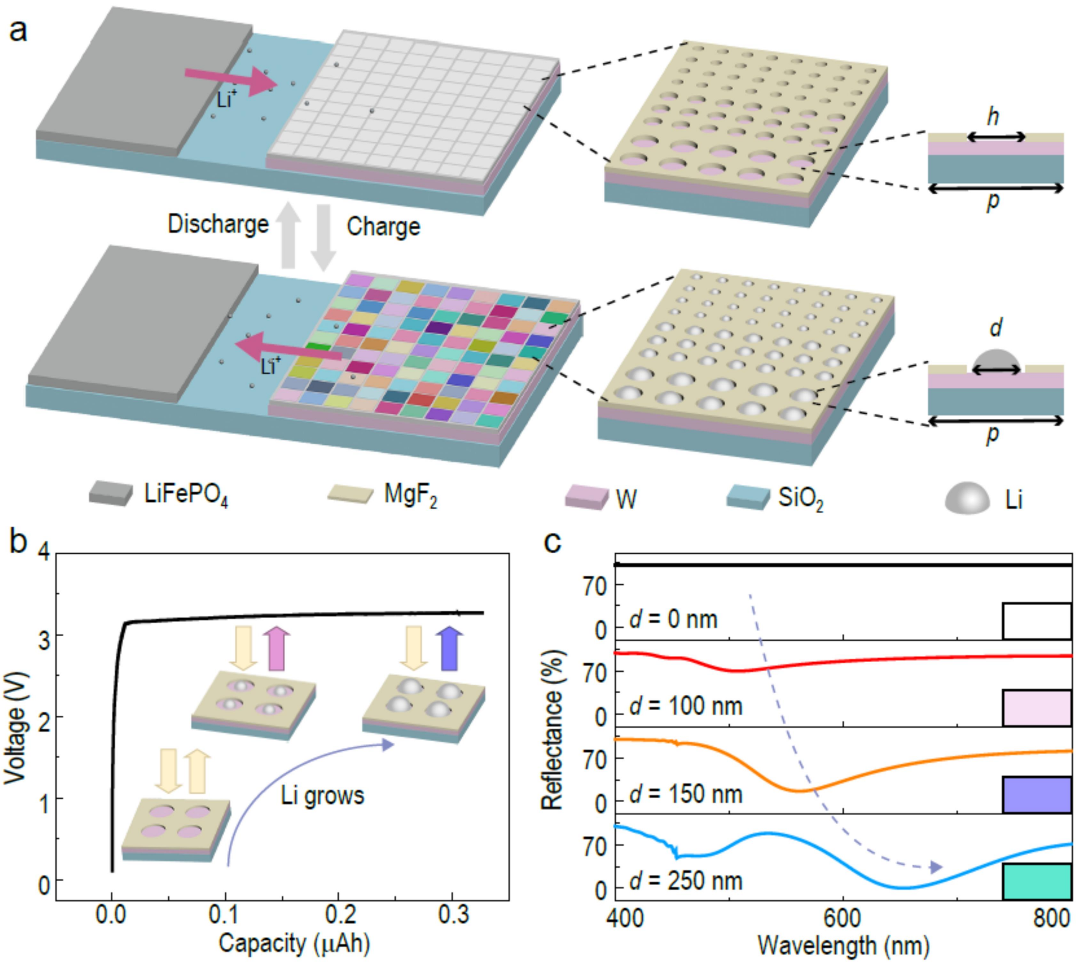

Fig. 1. The schematic and illustration of the low-powered dynamic plasmonic color display. (a) The schematic and working mechanism. The display panel which serves as the anode of the

battery is composed of silica (SiO_2) substrate, tungsten (W) conductive film (100 nm thick) and magnesium fluoride (MgF_2) insulating layer (30 nm thick) with periodic holes under the colorless "off" state. Each pixel is composed of periodic holes with a given lateral period (*p*) and diameter (*h*). During the charging (electrodeposition) process, Li nanoparticles with diameter (*d*) generate colors as the "on" state. These colors can be erased during the discharging process once Li nanoparticles are stripped off. (b) The voltage profile of the dynamic system as a function of charging capacity during the charging process. Insets show the evolution of Li structures and reflection colors. (c) The simulated reflection spectra as a function of the diameter (*d*) of Li metal nanoparticles (with constant lateral period p = 320 nm) and the corresponding colors (on the right).

The correlation between the optical parameters for color display (the reflection spectra in visible and corresponding colors) and the electrochemical parameters for battery (the applied voltage and electric capacity) is established (Figs. 1a-c). Fig. 1b depicts the battery voltage and qualitative structural evolution profiles of Li metal nanoparticles as a function of the capacity (note: capacity is defined as the product of current density and time). Li metal nanoparticles grow as the charging capacity increases, which changes the reflection spectral response, resulting in the real-time plasmonic coloration (schematically depicted in the insets in Fig. 1b). Based on systematic simulations (see METHODS and Supplementary Fig. 3 for details), Fig. 1c further illustrates the quantitative correlation between the evolved Li nanoparticle sizes (refer to the charging capacity) and reflection spectral responses, as well as the corresponding reflection colors. Detailed theoretical analyses on absorption cross section (Supplementary Fig. 4) and electric field distribution profiles (Supplementary Fig. 5) reveal that, localized surface plasmon resonance (LSPR) of the as-grown isolated Li nanoparticles instead of the surface diffraction modes of periodic structures plays the crucial roles for the plasmonic color generation.

Electrochemical tunability of Li metal-based plasmonic multi-colors

A more comprehensive demonstration of the electrochemical tunability of Li plasmonic color is experimentally illustrated in Fig. 2a. To precisely tune the structural colors, periodic nanoholes (period *p*, hole diameter *h*) were prepared onto the electrode by the electron beam lithography (EBL) for the electric-driven Li metal deposition. In order to render a broad-range palette of colors, stepwise tuning of the charging capacity was employed for a gradual increment of Li nanoparticle size (*d*). The pixel colors shown in Fig. 2a are functions of geometry parameters (*p*: 200 - 440 nm, *h*: 120 - 320 nm) and deposition capacity (0 – 0.35 μAh), which are derived from measured optical images of the structured anodes by arbitrarily getting the RGB values using color picker in software Photoshop (see Supplementary Fig. 8). The top part of Fig. 2a demonstrates that at the beginning depositing state, *h* determines the color because *h* affects the size of the Li nanoparticle (*d*) which plays a crucial role in the LSPR mode color generation, while at the later charging state, *p* also affects the color because as Li particles grow the electromagnetic field of each nanoparticle overlaps and the impact of *p* can not be ignored (more discussions are shown in Supplementary Fig. 6). One may find that plasmonic colors of a wide color gamut can be enabled with patterned Li nanoparticles by fine-tuning particle sizes and charging capacity (Fig. 2a), revealing the capability of multi-color dynamic control.

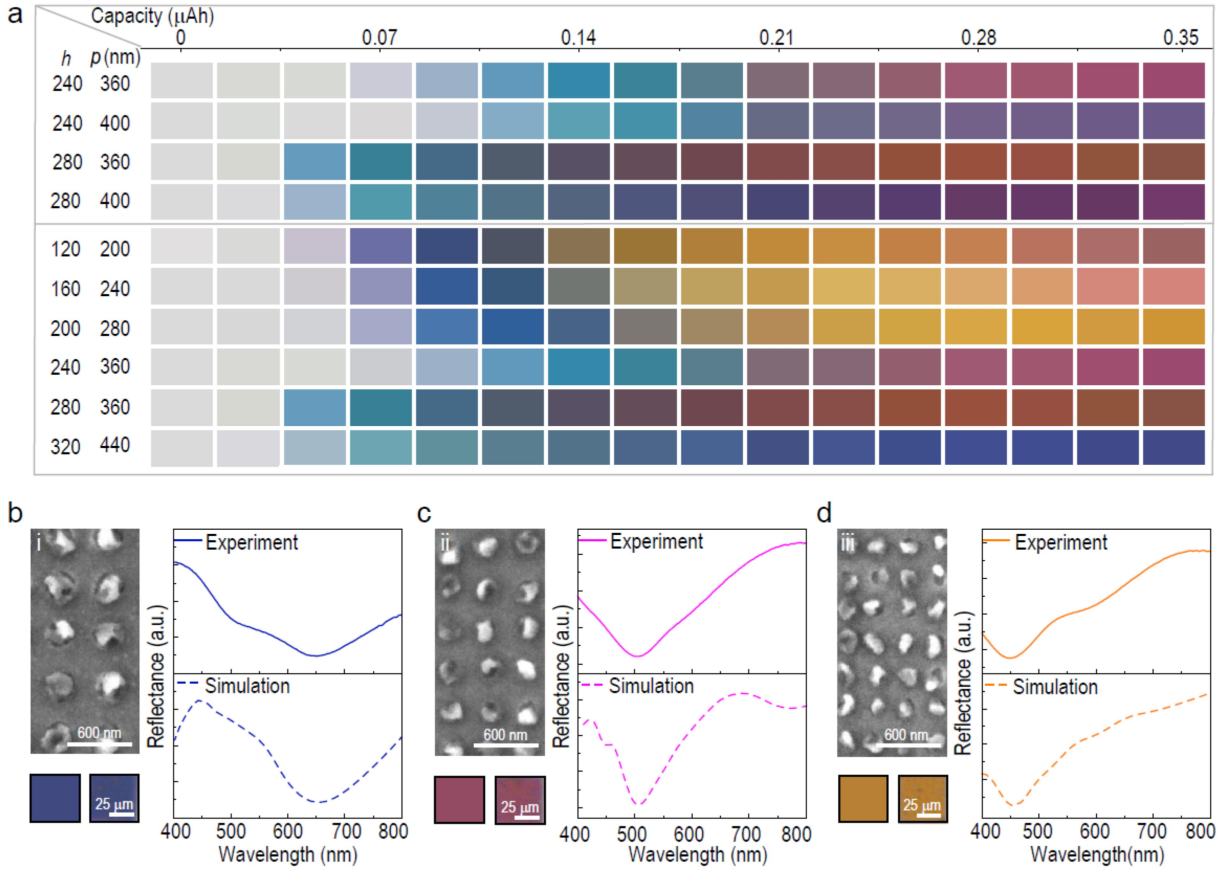

Fig. 2. Structural dependence of the Li-based plasmonic color display. (a) The capacity-dependent structural color panels derived from microscopic images of Li patterns with different lateral periods *(p)* and hole diameters *(h)* during coloration. (b-d) Measured and simulated reflectance spectra of three representative structural colors as well as relevant SEM and color patches (the left color are derived from the right microscope image): (i) p = 440 nm, d = 280 nm, h=280 nm, (ii) p = 360 nm, d = 240 nm, h=180 nm, and (iii) p = 280 nm, d = 160 nm, h=160 nm, respectively.

We further exhibit three representative plasmonic colors of different Li patterns by running the electrodeposition experiments for a fixed charging capacity of about 0.33 μAh, as shown in Figs. 2b-d. In these pixels, the diameters of deposited Li nanoparticles are 280 nm, 240 nm and 160 nm (measured from the ex-situ SEM images i, ii and iii of Figs. 2b-d) for blue, red and yellow colors, with measured reflectance dip at 650 nm, 500 nm and 450 nm, respectively. The simulated reflection spectra of the Li patterns (with parameters retrieved from the ex-situ SEM images) agree well with the measured ones, which confirms the plasmon-enabled color generation.

Dynamic plasmonic color displays

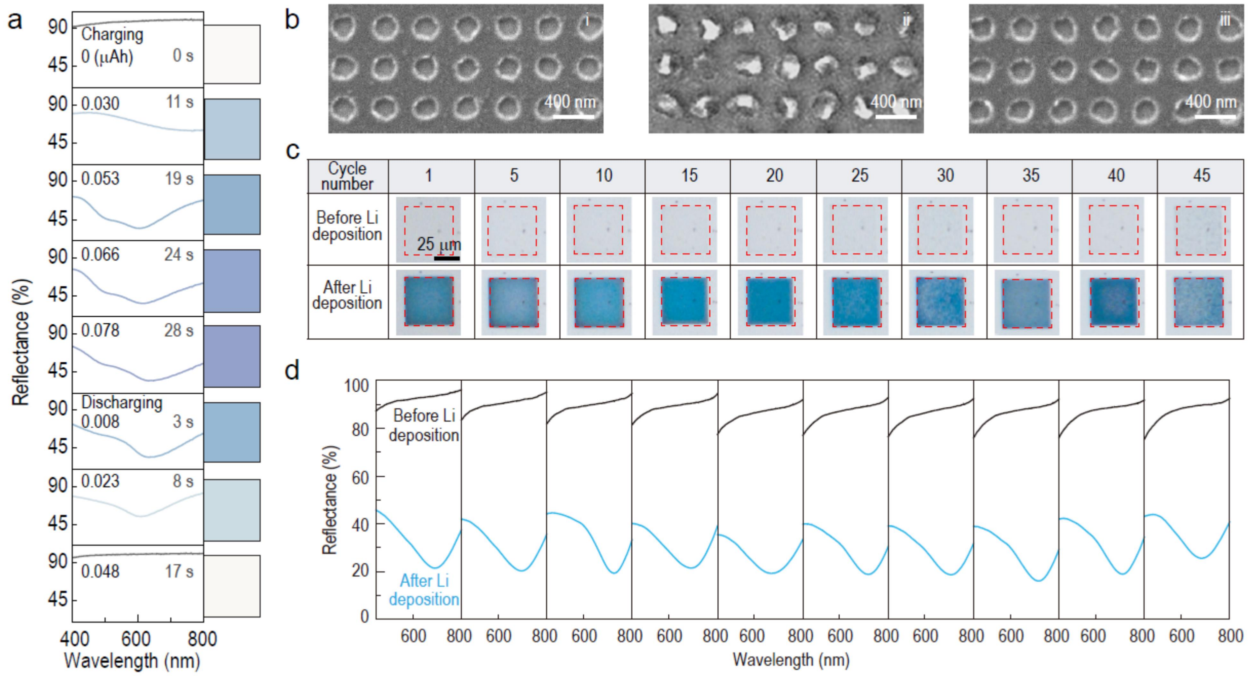

Fig. 3. Dynamic plasmonic color displays and the cycling performance. (a) A complete generating/erasing cycle of blue color characterized by the measured reflectance spectra and derived colors. (b) SEM images of the blue color display panel (p = 400 nm, h =200 nm) at the original (i), color generation (ii), and color erasure (iii) states during one cycle. (c-d) Cycling performance of a dynamic blue coloration: optical images (c), the correlated reflectance spectra (d).

As the built-in structural transformation and reflectance tunability is confirmed, we further demonstrate the capability of electric-driven dynamical coloration. To evaluate the cycling performance of the structural color display, we perform the in-situ measurements on reflectance spectra of the representative blue color (p = 400 nm, h = 200 nm), as shown in Fig. 3. During the in-situ charging/discharging experiment, the measured reflectance spectra evolve from the initial colorless state (with nearly 100% reflectance in the visible regime) gradually to the state of different shades of blue colors (with reflection dips at around 600 nm). It finally recovers to the original state with nearly 100% reflectance in the visible regime after a complete cycle (Fig. 3a). The corresponding ex-situ morphologies of the display panel during the original, color generation and color erased states are shown in Fig. 3b. After the charging process with the generated structure color, Li nanoparticles are precisely deposited into the holes (Fig. 3b(ii)). As the color erasing process is terminated in the discharging process, the deposited Li nanoparticles are fully removed with the empty holes recovered (Fig. 3b(iii)), which validates the reversible structural transformation and thus dynamic colors of Li nanoparticles as suggested in Fig. 1.

To evaluate the cycling performance of the dynamic plasmonic color display, we test the reflectance spectra of the “on/off” coloration for at least 45 cycles via repeatable charging and discharging processes, as shown in Figs. 3c-d. The blue color is well maintained at the color generation states (or “on” state after Li deposition) and fully removed at the “off” states (before Li deposition) during long cycling (Fig. 3c). The considerable optical contrast (> 50% intensity of reflectance dip) and wavelength of reflectance dip (around 700 nm) at coloration states are repeatable during cycles (Fig. 3d). The overall cycling performance makes it a promising candidate for the dynamic color display.

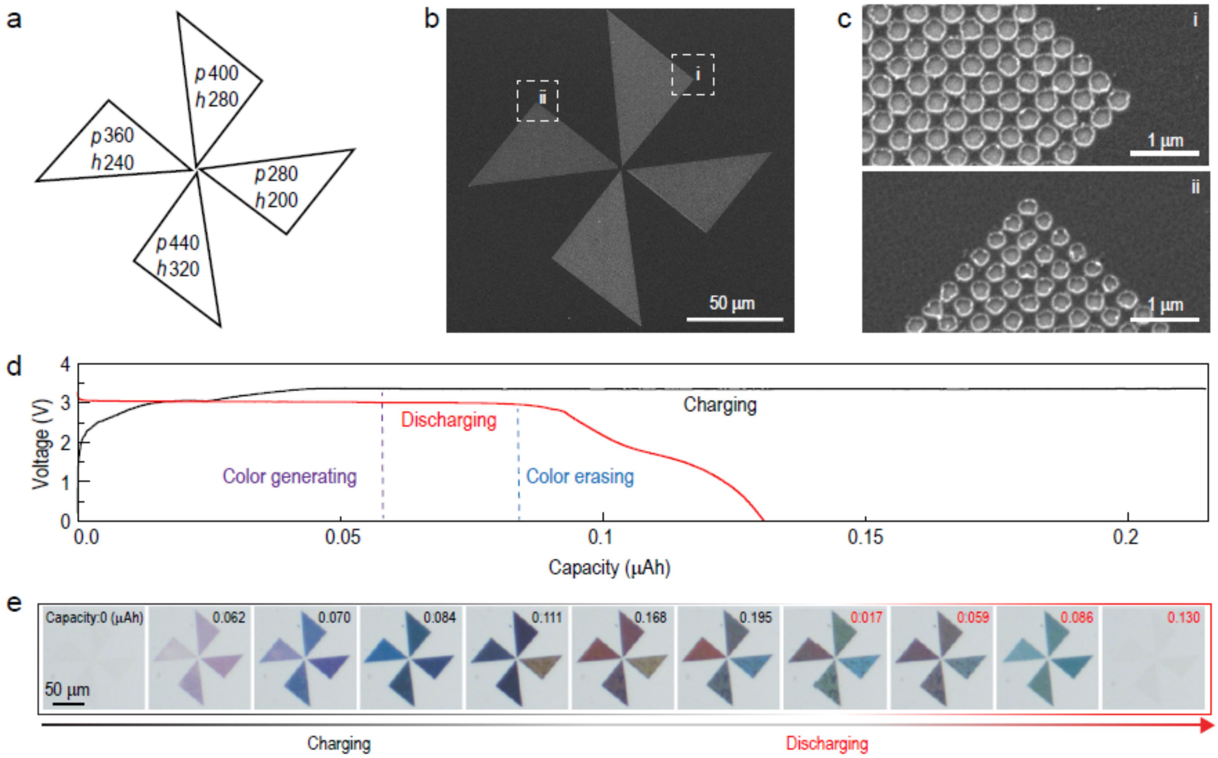

Fig. 4. Plasmonic animations of a chromatic windmill pattern. (a) Design of a color display panel - a windmill pattern. (b-c) Overview and enlarged SEM images of the windmill pattern. (d) The battery voltage profile during charging and discharging processes. (e) The dynamic process of the plasmonic animation during charging and discharging processes for color generating and erasing, corresponding to the charging capacity (labeled upper black numbers, μAh) and discharging capacity (labeled upper red numbers, μAh).

To further unravel the dynamic tunability of multiple structural colors, we have designed a plasmonic animation of a chromatic micro-windmill over full cycling, with schematic and SEM images shown in Figs. 4a-c, respectively. The pattern geometries of the four regions are carefully designed with geometry parameters labeled in Fig. 4a. The charging and discharging current densities of about 0.4 mA cm^{-2} and 0.2 mA cm^{-2} are applied respectively (see Fig. 4d for the voltage profile). Fig. 4e illustrates the real-time animation of the chromatic windmill (purple, blue, red, and yellow) over the charging/discharging capacity. A series of color generation takes place within 0.062 μAh. Subsequently, the color of the windmill changes as a function of the charge capacity (until 0.195 μAh). During the discharging process, the colors of the windmill are completely erased after discharging capacity of 0.130 μAh. Furthermore, an electric-driven micro-animation of a flying butterfly is demonstrated as well (Movie S1 and Supplementary Fig. 10). It indicates that this dynamic color display can be well programmed by the applied electrical signals, exhibiting compatibility with versatile smart electronic devices.

Low-powered dynamic plasmonic color display

Finally, we demonstrate the low-powered nature of the proposed lithium plasmon based dynamic display device with rational electronic designs such as employing one pixel panel to charge another and vice versa, one of the low-powered strategies of which is shown in Fig. 5a. The proposed proof-of-concept device can consist of a large number of plasmonic color pixels (or mini-batteries, noted as the colored boxes in Fig. 5a), partial of which are operating at the color erasing states (in discharging process) while others are at color generating states (in charging process). In detail, for an arbitrary plasmonic pixel (noted as i), once it experiences the discharging process, the output power can lighten up the LED until the stored energy (see the lower photos of the left panel in Fig. 5b) is exhausted while the electrically driven structure transformation can simultaneously result in a capacity dependent color evolution (see the upper photos of the left panel in Fig. 5b), unraveling the dual functionalities of information and energy of each pixel (details are shown in the Supplementary Fig. 14).

To further enable the energy recycling of the overall display panel and realize a low-powered display, we take an arbitrary pair of pixels for demonstration. As depicted in the right panel of Fig. 5b, the colored pixel (i) with stored energy can recharge and power the other pixel (j) without external power input. During these processes, each pixel (i and j) can output an independent time-resolved color (as information carriers) while energy consumed by each pixel will be recycled by its counterpart via the reversed electrochemical process (see Supplementary Fig. 15 for experimental details). Note that, the two-versus-one-pixel cycling configuration employed in Supplementary Fig. 15 is just a simplified case to compensate for the overpotential mismatch during an entire cycling process. However, it is definitely unnecessary provided that more dedicated DC-DC voltage conversion strategies (widely employed in commercial electronic devices) are applied to enable a one-versus-one pixel configuration.

With clearly identified dual functionalities of these independent pixels (both as basic elements for color information and micro-power-supplier for the display), one can quantitatively evaluate the energy consumption of the integrated display device. A direct comparison of the energy consumption of our work with representative commercial display devices is depicted in Fig. 5c. Taking the average energy efficiency (~ 56.70%) of our prototype device, for example, the specific energy consumption is ~ 0.390 mW cm^{-2} without optimization, which is at least one order of magnitude lower than the commercial active matrix organic light-emitting diode (AMOLED) (at the brightness of 160 cd cm^{-2} and Contrast Ratio of 10000:1) or several times lower than the electronic paper display (EPD) system [37,47]. Moreover, if the display is operated at a static coloration state, the specific energy consumption can be even three times lower (0.105 mW cm^{-2}, see METHODS for detailed explanations). In addition, aiming at the intersection of plasmonics and energy storage, this technology will benefit from promising advancements in both fields. For instance, once the energy efficiency of the Li metal battery system reaches the mainstream commercial batteries (~ 99.00%), the overall energy consumption can be reduced down to 0.009 mW cm^{-2}, which suggests a power reduction of about three orders than the commercial AMOLED (Fig. 5d).

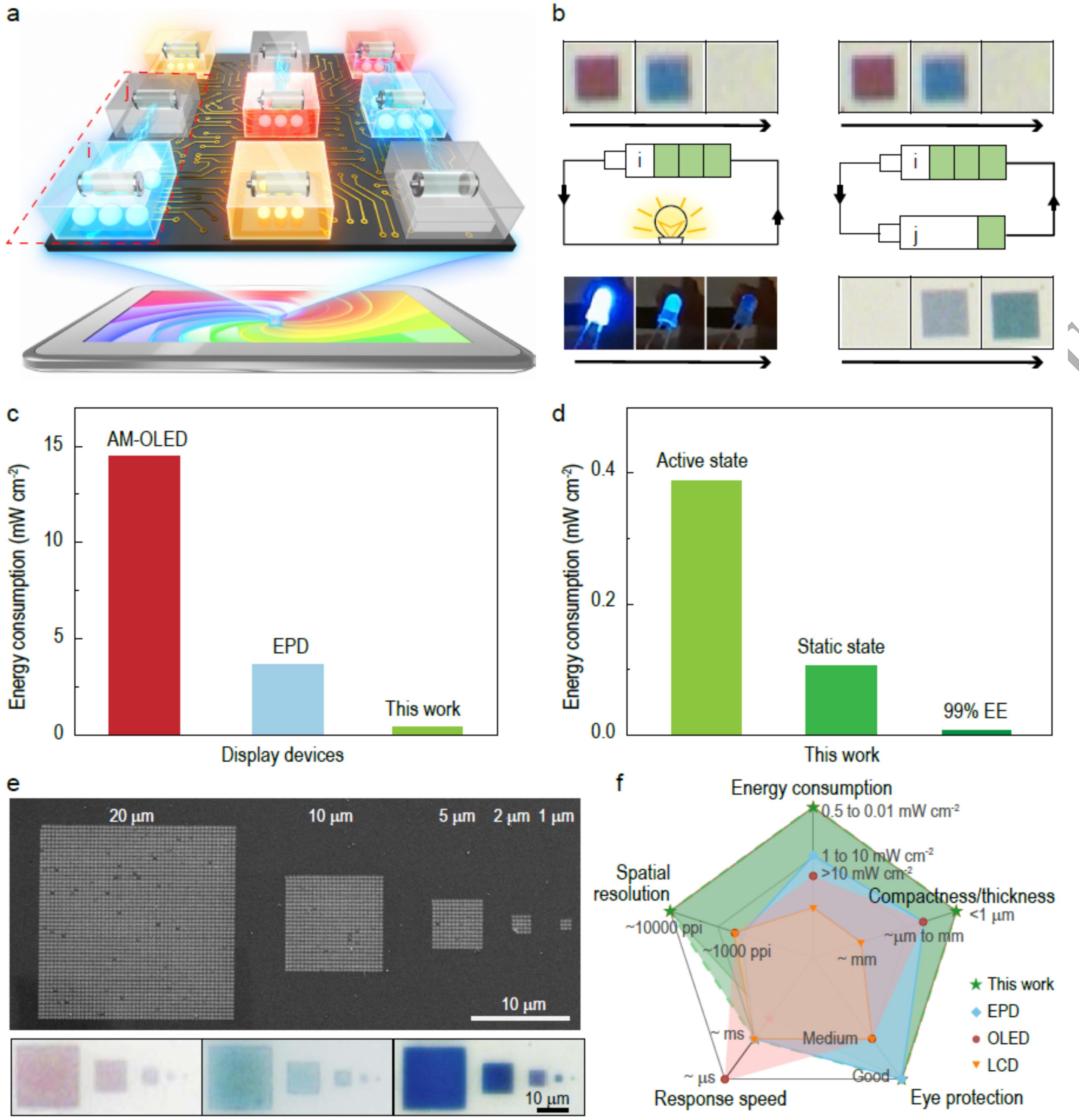

Fig. 5. Low-powered dynamic plasmonic color display. (a) The operation schematic of the low-powered dynamic plasmonic color display: Display contains many pixels with some pixels erasing color and some generating color, so the color erasing pixels with stored energy (eg. pixel i) can recharge and power other pixels (eg. pixel j) for color generation. (b) The dual functionalities of the power supplier and information display of the device. (c, d) The comparisons of energy consumption of different display devices [37,47]. The energy

consumption of the proposed proof-of-concept device is evaluated as ~ 0.390 mW cm^{-2} at the active coloration state for around 56.70% energy efficiency (EE) and ~ 0.105 mW cm^{-2} at the static coloration state, even lower to ~ 0.009 mW cm^{-2} for 99.00% EE in the future. (e) SEM and optical images of pixels with different sizes (20 μm, 10 μm, 5 μm, 2 μm, 1 μm) for different colors. (f) The comparison of different display technologies in spatial resolution, energy consumption, response speed, compactness/thickness, and eye protection. [37, 47-50]

Finally, the pixel-scaling limit of the proposed lithium plasmonic device is experimentally evaluated and shown in Fig. 5e and Supplementary Fig. 16. Full-color pixels with different sizes (decreasing from 20 μm to 1 μm) and different colors in a square shape can be observed using a conventional optical microscope, unraveling that the full-color pixel size can be down to 1 μm even in the complicated liquid surroundings (~ less than one half of that of metasurface counterpart reported thus far [8]). This enables a pronounced high spatial resolution of electrically dynamic color display, which is one order magnitude higher than the resolution of current displays (~1000 PPI) (eg. LCD, LED, EPD, etc.) even in the rather complicated liquid environment [48, 50].

As a systematic evaluation of the proposed lithium plasmon based dynamic display, we compare this work with different display technologies in five representative parameters, including spatial resolution, energy consumption, response speed, compactness/thickness, and eye protection in the radar chart in Fig. 5f. Benefiting from the light field manipulation beyond the diffraction limit and the energy storage battery of lithium metals, this work shows much lower energy consumption, much higher spatial resolution, higher compactness, considerable modulation speed and good eye protection for the full-color display.[37, 47-50] Thus, this Li metal based plasmonic color display shows the best overall performance, opening up a promising direction for the future high-performance display technology, especially in the application of augmented reality.

CONCLUSION

In summary, we demonstrate a low-powered Li metal based plasmonic device, with dual functionalities of the electric-driven color display and the energy recycling unit. Li metal nucleates, grows, and strips on the precisely patterned anode inside the Li metal battery, leading to the generation, change, and erasure of plasmonic colors for the dynamic color display. The plasmonic feature of lithium metals makes the display device of rather high spatial resolution while the energy storage feature of the Li metals essentially lowers the energy consumption of the dynamic plasmonic color display to 0.390 mW cm^{-2} for the dynamic and 0.105 mW cm^{-2} for the static coloration. Converging Li metal plasmonics as both the information carrier (plasmonic material) and energy carrier (battery anode), this technique will benefit from the advancement of both fields to provide a promising strategy towards energy-efficient and high resolution integrated photonic platforms.

METHODS

Fabrication of the Li metal-based dynamic plasmonic color display system

The Li metal-based dynamic plasmonic color display device is a planar anode-free Li metal battery. It consists of three parts: nanostructured anode, liquid electrolyte and cathode. The anode template was fabricated through EBL with the following steps as demonstrated in Supplementary Fig. 1. A detailed description of this fabrication is available in Supplementary data.

Characterization

The optical color images and dynamic animation were obtained using a brightfield reflection microscopy (Nikon) illuminated by a light source (Energetiq Laser-Driven Light Source, EQ-99). A digital charge-coupled device (CCD) Camera (Allied-Vision Prosilica GT2450C) was used to capture the color micrographs with a 20 × (NA ¼ 0.4) objective. The optical reflection spectra were measured in reflection mode using a microspectrometer (CRAIC) with the electric field of the unpolarized light in the plane with the substrate surface. The measured reflectance spectra were normalized with respect to that of a bare region ($MgF_2/W/SiO_2$ flat film soaking in the electrolyte) next to the periodic hole structures.

An electrochemical workstation (Biologic SP-20) was used to control the Li nanoparticles deposition/stripping during the charging and discharging processes through galvanostatic cycling and measure the time-dependent potentials. The morphologies and structures of the dynamic display panels at the beginning, coloration, and color erasing states were characterized by SEM (Tescan Mira3). For the characterization of Li morphologies after the electrochemical deposition/stripping, the display device was disassembled in the Ar-filled glove box after optical reflectance measurement, then rinsed with fresh diethyl carbonate and dried. Display panels were mounted onto SEM stages and sealed in Ar-filled transfer vessels for immediate SEM observation to avoid oxidation of Li metal.

Numerical simulations

The finite-difference time-domain method was used to calculate the reflection spectrum. For simplicity, periodic boundary condition and plane wave as the excitation source were used for the modeling. The material parameters of Li metal and tungsten were from the Palik data, and the refractive index of SiO_2 substrate, MgF_2 insulating layer and electrolyte were set as 1.45, 1.38 and 1.4, respectively. In order to simplify the simulations, the morphology of deposited Li metal was set as hemispheres with the diameter (d). The period (p) was set from 200 nm to 440 nm. The thicknesses of SiO_2 substrate, W conductive layer, MgF_2 insulating layer and electrolyte layer were 1 mm, 100 nm, 30 nm and 1 μm, respectively.

Chromaticity calculation

We calculated the color of the deposited Li metal hemispheres according to the International Commission on Illumination (CIE) "standard observer" functions based on human data, the details are available in Supplementary data.

Energy consumption calculation

The energy consumption of our plasmonic display during the display is calculated with the following formulation:

$$P = \overline{U_c} I_c (1 - EE).$$

Here, $\overline{U_c}$ is the average charge voltage, I_c is the charge current, EE is energy efficiency which is the ratio of the discharged energy to the charged energy. The detailed calculations are shown in Supplementary data.

SUPPLEMENTARY DATA

Supplementary data are available at NSR online.

ACKNOWLEDGMENTS

We acknowledge the micro-fabrication center of National Laboratory of Solid State Microstructures (NLSSM) for technique supports. J.Z. acknowledges the support of Explorer Prize.

FUNDING

This work was supported by the National Key Research and Development Program of China (2021YFA1400700), the National Natural Science Foundation of China (12022403, 51925204, 61735008, and 11874211) and the Excellent Research Program of Nanjing University (ZYJH005).

AUTHOR CONTRIBUTIONS

L.Z. and J.Z. proposed the research. Y.J. and J.L. designed the experiments. J.L. and Y.J. contributed equally to this work. J.L. and Y.J. finished the sample fabrication, electrochemical measurement, optical measurement, SEM characterization, numerical simulations and data analysis. Y.Z., X.C., Y.J., H.M. and H.Y. helped the sample fabrication. P.H. and J.L. performed the chromaticity calculations. S.Z., T.X. and B.Z. participated in data analysis and discussion. J.L., Y.J., L.Z., and J.Z. wrote the paper with input from all authors.

Conflict of interest statement. None declared.

REFERENCES

1. Burroughes JH, Bradley DDC and Brown AR *et al.* Light-emitting diodes based on conjugated polymers. *Nature* 1990; **347**: 539-541.
2. Dunn B, Kamath H and Tarascon JM. Electrical energy storage for the grid: a battery of choices. *Science* 2011; **334**: 928-935.
3. Lin D, Liu Y and Cui Y. Reviving the lithium metal anode for high-energy batteries. *Nat. Nanotechnol.* 2017; **12**: 194-206.
4. Huang Y, Hsiang EL and Deng MY *et al.* Mini-LED, Micro-LED and OLED displays: present status and future perspectives. *Light Sci. Appl.* 2020; **9**: 105.
5. Fusella MA, Saramak R and Bushati R *et al.* Plasmonic enhancement of stability and brightness in organic light-emitting devices. *Nature* 2020; **585**: 379-382.
6. Wang Y, Nie H and Han J *et al.* Green revolution in electronic displays expected to ease energy and health crises. *Light Sci. Appl.* 2021; **10**: 33.
7. Joo WJ, Kyoung J and Esfandyarpour M *et al.* Metasurface-driven OLED displays beyond 10,000 pixels per inch. *Science* 2020; **370**: 459-463.
8. Hopmann E and Elezzabi AY. Plasmochromic nanocavity dynamic light color switching. *Nano Lett.* 2020; **20**: 1876-1882.

9. Li H, Firby CJ and Elezzabi AY. Rechargeable aqueous hybrid Zn^{2+}/Al^{3+} electrochromic batteries. *Joule* 2019; **3**: 2268-2278.

10. Xu W, Wang JL and Ding F *et al.* Lithium metal anodes for rechargeable batteries. *Energy Environ. Sci.* 2014; **7**: 513-537.

11. Yabuuchi N, Kubota K and Dahbi M *et al*. Research development on sodium-ion batteries. *Chem. Rev.* 2014; **114**: 11636-11682.

12. Cheng XB, Zhang R and Zhao CZ. *et al.* Toward safe lithium metal anode in rechargeable batteries: a review. *Chem. Rev.* 2017; **117**: 10403-10473.

13. Chen X, Chen Y and Ma Z *et al.* How is energy consumed in smartphone display applications? *In Proc. ACM 14th Workshop Mobile Comput. Syst. Appl. (HotMobile)* 2013; 3.

14. Pasricha S, Luthra M and Mohapatra S *et al.* Dynamic backlight adaptation forlow-power handheld devices. *IEEE Des. Test* 2014; **21**: 398–405.

15. Yan Z and Chen CW. Too many pixels to perceive: subpixel shutoff for display energy reduction on OLED smartphones. *In Proceedings of the 2017 ACM on Multimedia Conference (MM ’17)* 2017; 717–725.

16. Carroll A and Heiser G. An analysis of power consumption in a smartphone. *USENIX annual technical conference, Boston, MA* 2010; **14**: 21.

17. Jin Y, Liang J and Wu S *et al.* Electrical dynamic switching of magnetic plasmon resonance based on selective lithium deposition. *Adv. Mater.* 2020; **32**: 2000058.

18. Jin Y, Zhou L and Yu JY *et al.* In operando plasmonic monitoring of electrochemical evolution of lithium metal. *Proc. Natl. Acad. Sci. U S A* 2018; **115**: 11168-11173.

19. Wang Y, Yu JY and Mao YF *et al.* Stable, high-performance sodium-based plasmonic devices in the near infrared. *Nature* 2020; **581**: 401-405.

20. Blaber MG, Arnold MD and Harris N *et al.* Plasmon absorption in nanospheres: a comparison of sodium, potassium, aluminium, silver and gold. *Physica B: Condens. Matter.* 2007; **394**: 184-187.

21. Blaber MG, Arnold MD and Ford MJ. Designing materials for plasmonic systems: the alkali-noble intermetallics. *J. Phys. Condens. Matter.* 2010; **22**: 095501.

22. Boltasseva A and Atwater HA. Low-loss plasmonic metamaterials. *Science* 2011; **331**: 290-291.

23. Shao L, Zhuo X and Wang J. Advanced plasmonic materials for dynamic color display. *Adv. Mater.* 2018; **30**: e1704338.

24. Kumar K, Duan HG and Hegde RS *et al.* Printing colour at the optical diffraction limit. *Nat. Nanotechnol.* 2012; **7**: 557-561.

25. Kristensen A, Yang JKW and Bozhevolnyi SI *et al.* Plasmonic colour generation. *Nat. Rev. Mater.* 2016; **2**: 16088.

26. Xu T, Wu YK and Luo X *et al.* Plasmonic nanoresonators for high-resolution colour filtering and spectral imaging. *Nat. Commun.* 2010; **1**: 59.

27. Neubrech F, Duan X and Liu N. Dynamic plasmonic color generation enabled by functional materials. *Sci. Adv.* 2020; **6**: eabc2709.

28. Goh XM, Zheng Y and Tan SJ *et al.* Three-dimensional plasmonic stereoscopic prints in full colour. *Nat. Commun.* 2014; **5**: 5361.

29. Kim I, Jang J and Kim G *et al.* Pixelated bifunctional metasurface-driven dynamic vectorial holographic color prints for photonic security platform. *Nat. Commun.* 2021; **12**: 3614.

30. Jang J, Badloe T and Sim YC *et al.* Full and gradient structural colouration by lattice amplified gallium nitride Mie-resonators. *Nanoscale* 2020; **12**: 21392-21400.

31. Zhang C, Jing J and Wu Y *et al.* Stretchable all-dielectric metasurfaces with polarization-insensitive and full-spectrum response. *ACS Nano* 2020; **14**: 1418-1426.

32. Kim I, Yun J and Badloe T *et al.* Structural color switching with a doped indium-gallium-zinc-oxide semiconductor. *Photonics Res.* 2020; **8**: 1409-1415.

33. Ko B, Chae JY and Badloe T *et al.* Multilevel absorbers via the integration of undoped and tungsten-doped multilayered vanadium dioxide thin films. *ACS Appl. Mater. Interfaces* 2022; **14**: 1404-1412.

34. Liu J, Feng K and Wang Y *et al.* High-color-purity, high-brightness and angle-insensitive red structural color. *Chin. Opt. Lett.* 2022; **20**: 021601.

35. Jang J, Badloe T and Yang Y *et al.* Spectral modulation through the hybridization of Mie-scatterers and quasi-guided mode resonances: realizing full and gradients of structural color. *ACS Nano* 2020; **14**: 15317-15326.

36. Wang G, Chen X and Liu S *et al.* Mechanical chameleon through dynamic real-time plasmonic tuning. *ACS Nano* 2016; **10**: 1788-1794.

37. Xiong K, Emilsson G and Maziz A *et al.* Plasmonic metasurfaces with conjugated polymers for flexible electronic paper in color. *Adv. Mater.*2016; **28**: 9956-9960.

38. Tsuboi A, Nakamura K and Kobayashi N. A localized surface plasmon resonance-based multicolor electrochromic device with electrochemically size-controlled silver nanoparticles. *Adv. Mater.* 2013; **25**: 3197-3201.

39. Duan X, Kamin S and Liu N. Dynamic plasmonic colour display. *Nat. Commun.* 2017; **8**: 14606.

40. Duan X and Liu N. Scanning plasmonic color display. *ACS Nano* 2018; **12**: 8817-8823.

41. Wu Y, Yang W and Fan Y *et al.* TiO2 metasurfaces: from visible planar photonics to photochemistry. *Sci. Adv.* 2019; **5**: eaax0939.

42. Gao Y, Huang C and Hao C *et al.* Lead halide perovskite nanostructures for dynamic color display. *ACS Nano* 2018; **12**: 8847-8854.

43. Li Y, van de Groep J and Talin AA *et al.* Dynamic tuning of gap plasmon resonances using a solid-state electrochromic device. *Nano Lett*. 2019; **19**: 7988-7995.

44. Peng JL, Jeong HH and Lin QQ *et al.* Scalable electrochromic nanopixels using plasmonics. *Sci. Adv.* 2019; **5**: eaaw2205.

45. Xu T, Walter EC and Agrawal A *et al.* High-contrast and fast electrochromic switching enabled by plasmonics. *Nat. Commun.* 2016; **7**: 10479.

46. Sun S, Yang W and Zhang C *et al.* Real-time tunable colors from microfluidic reconfigurable all-dielectric metasurfaces. *ACS Nano* 2018; **12**: 2151-2159.

47. Fernández M, Casanova E and Alonso I. Review of display technologies focusing on power consumption. *Sustainability* 2015; **7**: 10854-10875.

48. Comiskey B, Albert JD and Yoshizawa H *et al.* An electrophoretic ink for all-printed reflective electronic displays. *Nature* 1998; **394**: 253-255.

49. Li JJ, Nie XM and Zhen W *et al.* New developments and comparisons in display technology. *Chinese J. of Liq. Cryst. Disp.* 2018; **33**: 74-84.

50. Chen HW, Lee JH and Lin BY *et al.* Liquid crystal display and organic light-emitting diode display: present status and future perspectives. *Light Sci. Appl.* 2018; **7**: 17168.